Review of Scientific Instruments

Laser ultrasonic measurements to estimate the elastic properties of rock samples under *in situ* conditions

Cite as: Rev. Sci. Instrum. **90**, 114503 (2019); https://doi.org/10.1063/1.5120078
Submitted: 16 July 2019 . Accepted: 30 October 2019 . Published Online: 21 November 2019

Jonathan Simpson, Kasper van Wijk, Ludmila Adam, and Caitlin Smith

Review of Scientific Instruments ARTICLE scitation.org/journal/rsi

Laser ultrasonic measurements to estimate the elastic properties of rock samples under *in situ* conditions

Cite as: Rev. Sci. Instrum. 90, 114503 (2019); doi: 10.1063/1.5120078
Submitted: 16 July 2019 • Accepted: 30 October 2019 •
Published Online: 21 November 2019

Jonathan Simpson,[1,2,a] Kasper van Wijk,[1,2] Ludmila Adam,[3] and Caitlin Smith[2]

AFFILIATIONS

[1]The Dodd-Walls Centre for Photonic and Quantum Technologies, Auckland 1010, New Zealand
[2]Physical Acoustics Laboratory, Department of Physics, The University of Auckland, Auckland 1010, New Zealand
[3]Physics of Rocks Laboratory, School of Environment, The University of Auckland, Auckland 1010, New Zealand

[a]**Electronic mail:** jsim921@aucklanduni.ac.nz

ABSTRACT

We present a new noncontact methodology to excite and detect ultrasonic waves in rocks under *in situ* pressure and temperature conditions. Optical windows in the side of a pressure vessel allow the passage of a laser source and a receiver for noncontact laser ultrasonic measurements. A heating mantle controls the temperature, and a rotational stage inside the vessel makes it possible to obtain measurements as a function of angle. This methodology is the first to combine the advantages of laser ultrasonics (LUS) over traditional transducer methods with measurements under *in situ* pressure and temperature conditions. These advantages include the absence of mechanical coupling, small sampling area, and broadband recordings of absolute displacement. After describing the experimental setup, we present control experiments to validate the accuracy of this new system for acquiring rock physics data. Densely sampled rotational scans performed on an Alpine Fault ultramylonite rock reveal a decrease in P-wave anisotropy from 62% at atmospheric pressure to 36% at 16 MPa. This result highlights the importance of performing rock physics measurements under *in situ* confining stress and demonstrates the advantages of the methodology for investigating anisotropy. In addition, a 5.6% decrease in the P-wave velocity of the ultramylonite sample between 20 °C and 100 °C at a constant 10 MPa confining stress demonstrates the capability of this new methodology for acquiring data under both *in situ* pressure and temperature conditions. This new methodology opens the door for probing the pressure and temperature dependence of the elastic properties of rocks and other materials using LUS techniques.

I. INTRODUCTION

Estimates of the elastic properties of materials are important in a wide range of fields, including medical imaging and structural engineering. In the field of rock physics, the elastic properties of rocks are studied in the lab to understand their dependence on both intrinsic features and environmental conditions.[1,2] The inferences drawn from these experiments are used to better understand geological processes, such as faulting.[3,4] As such, laboratory studies of rock elasticity over the past 70 years have created a valuable body of knowledge in solid earth geophysics.[1]

In the laboratory, the elastic properties of rocks are commonly determined by the pulse transmission experiment using ultrasonic transducers.[4–9] One or more ultrasonic transducers are coupled to the surface of a rock sample with glue or a liquid transducer couplant. A high voltage pulse applied across a piezoelectric crystal within the transducer creates a mechanical pulse, which propagates as an ultrasonic elastic wave (kilohertz-megahertz range) through the rock sample. A piezoelectric receiver converts the mechanical vibrations on the sample surface from these ultrasonic waves into an electrical signal.

Aside from piezoelectric transducers, other methods exist to generate and record ultrasonic elastic waves in a range of media. One such method requires no mechanical contact with the sample through the use of lasers. This method, known as laser ultrasonics (LUS), has been applied for investigating media with elastic waves for nondestructive testing,[10,11] medical imaging,[12] studies of wave propagation in heterogeneous media,[13,14] and rock physics,[15–17]

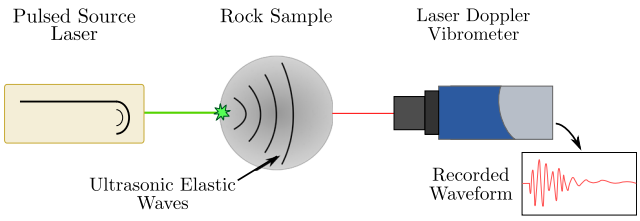

FIG. 1. With LUS, ultrasonic waves are excited at the surface of a rock sample by short high-energy laser pulses delivered to the surface by a pulsed source laser. A laser Doppler vibrometer detects the resulting vibrations on the opposite side of the sample.

among other applications. With LUS, transmitting and receiving transducers are replaced by a pulsed laser and a laser interferometer for the generation and detection of ultrasound (Fig. 1; see the work of Scruby and Drain[18] for a detailed treatment of LUS techniques), respectively. The pulsed laser delivers a short (<100 ns) pulse of electromagnetic radiation, usually in the infrared or visible spectrum, to the surface of the sample. This short high-intensity pulse causes thermoelastic expansion or ablation of the medium, generating ultrasonic waves which propagate through the sample. The resulting vibrations are detected at an arbitrary point on the sample surface by a laser interferometer, such as a laser Doppler vibrometer (LDV) reflecting a laser beam off the surface.[18]

LUS offers several advantages over traditional transducer methods for generating and recording elastic waves in laboratory rock samples.[19] First, the method is entirely noncontact. This eliminates the variability in sensitivity and bandwidth caused by the quality of the transducer coupling[18] and ensures that the LUS waveform contains only the response of the rock sample to the ultrasonic source. Moreover, the alignment of noncontact laser beams and their positioning on the sample can be adjusted (manually or under computer control) without touching the sample. The absence of mechanical contact also permits elastic wave measurements to be made at high temperatures. Previous studies have performed LUS measurements through the windows of a furnace at temperatures exceeding 1000 °C.[20–22] A second major advantage of the LUS method is the small area of the laser beams on the sample surface. Whereas the diameter of the contacting transducers is often the same order of magnitude as the wavelength at low-megahertz range ultrasound,[8,18] LUS laser beams have a diameter at least an order of magnitude smaller than the wavelength. Not only does this enable us to measure many independent propagation directions with different transects through a single sample, but it also guarantees that we unambiguously measure the group velocity.[8,15] A third major advantage of LUS for rock physics experiments is the broad bandwidth which can be generated and recorded (10^1–10^9 Hz).[19] The noncontact generation and detection is not bandwidth-limited by the physical dimensions of transducer elements.

Several studies have demonstrated the advantages of LUS over contacting transducers for performing laboratory rock physics measurements. Scales and Malcolm[13] studied wave propagation in granite samples with LUS techniques. Blum, Adam, and van Wijk[15] successfully used noncontact source and receiver lasers to estimate the elastic anisotropy and attenuation of reservoir shales. They obtained accurate anisotropy estimates by taking many independent measurements of the P- and S-wave velocities around cylindrical horizontal cores. Xie *et al.*[17] used this same technique for determining elastic anisotropy in organic-rich shales, using slight changes in the theoretical and experimental methods proposed by Xie *et al.*[16] to enhance reliability where LUS data are noisy. While these studies clearly demonstrate the advantages of noncontact LUS, they all share a common limitation: these measurements are performed on the benchtop at atmospheric pressure. Since the elastic properties of rocks vary significantly with confining stress (or more specifically, the difference between the external pressure and the pore fluid pressure),[23,24] obtaining realistic laboratory results requires performing measurements under conditions that replicate the *in situ* subsurface environment. To this end, ultrasonic transducer rock physics experiments are typically performed inside fluid-filled pressure vessels[5–7] or hydraulically driven triaxial rigs.[4,25]

Little work has been done to realize the full benefits of LUS techniques for realistic rock physics measurements under *in situ* conditions. Carson and Lebedev[26] extended the work of Lebedev *et al.*[25] by using an LDV to measure ultrasonic wave polarizations and velocities in a cubic rock sample under differential stress. However, an S-wave transducer glued to the sample surface was used for the ultrasonic source, and a stress could not be applied to one axis because two opposite faces had to be exposed for ultrasound generation and detection. We have developed an apparatus capable of performing LUS compressional wave measurements under isotropic confining stress and *in situ* temperatures. Rock samples are mounted inside a pressure vessel with two optical windows for the source and receiver laser beams. Adam *et al.*[27] presented pilot measurements using this apparatus at low pressure (0.8 MPa, or <100 m depth equivalent) in a single direction at a time. Since then, the system has extensively evolved.[28] Here, we present a detailed description of this apparatus and methodology, the first to combine the advantages of fully noncontact LUS with rock physics measurements under *in situ* conditions. Experimental validation is performed to establish the reliability of the methodology for acquiring accurate rock physics data. To demonstrate the implementation of this apparatus, we present rotational scans of an elastically anisotropic rock sample conducted from atmospheric pressure to 16 MPa. Additionally, we demonstrate initial measurements at *in situ* temperatures under confining stress.

II. EXPERIMENTAL SETUP

The primary component of the experimental setup for performing LUS under *in situ* conditions is a custom-made stainless steel pressure vessel with optical windows installed inside two diametrically opposite portals (Fig. 2). These optical windows are composed of 2.5 mm thick plugs of sapphire, allowing the source and receiver laser beams line-of-sight to the sample surface. The pressure vessel has a designed maximum pressure of 41 MPa (6000 psi) at which the maximum operating temperature is 200 °C. Isotropic confining pressure is currently provided by bottled nitrogen gas which has a maximum gauge pressure of 20 MPa. Gas pressure and flow rate are regulated and controlled via a manually operated needle valve. The pressure chamber has a volume of 4 l, but a series of stainless steel disks fill unused space within the vessel. Moreover, a 2.5 kW heating

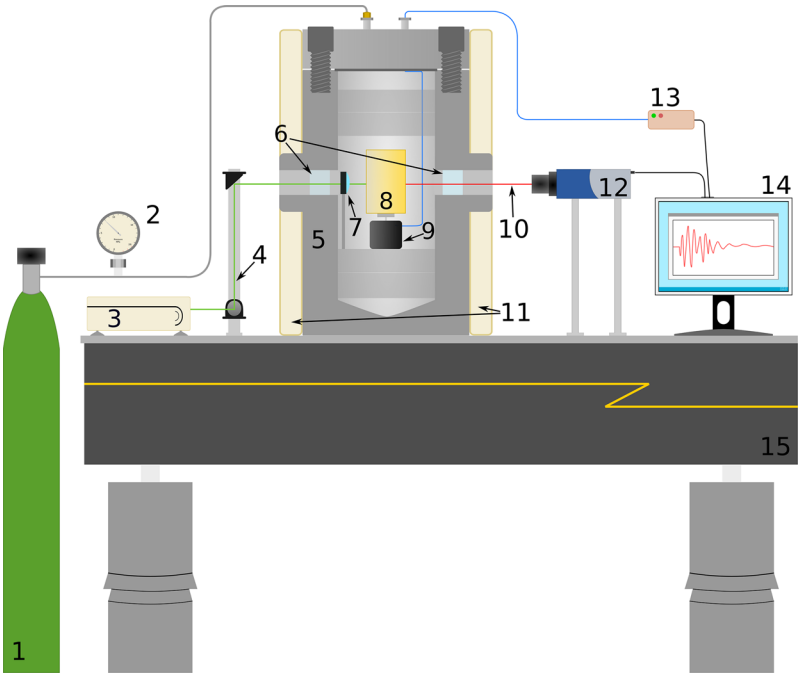

FIG. 2. Diagram showing the experimental setup. 1: High-pressure gas bottle. 2: Pressure gauge. 3: Pulsed source laser. 4: Infrared source laser beam. 5: Pressure vessel. 6: Optical windows. 7: Focusing lens. 8: Brass-jacketed rock sample. 9: Stepper motor. 10: Receiver laser beam. 11: Heating mantle. 12: Laser Doppler vibrometer. 13: Arduino motor controller and circuitry. 14: Control and acquisition PC. 15: Vibration isolated laser table. Diagram is not to scale.

mantle placed around the outside of the vessel is used to increase the temperature of the entire vessel and pressurized volume.

A Q-switched pulsed laser (Spectra-Physics Quanta-Ray INDI Nd:YAG) generates elastic waves with a 6–9 ns duration pulse of 1064 nm infrared light, 10 times per second. The laser light is almost entirely absorbed within tens of nanometers of the sample surface, resulting in rapid localized thermoelastic expansion of the material which acts as a source of ultrasonic waves.[18] We focus the beam to 3 mm in diameter and set the laser to deliver approximately 100 mJ per pulse in order to stay within the thermoelastic regime and prevent ablation. After propagating through and around the sample, the ultrasonic elastic waves are detected at the antipode of the source with a heterodyne laser Doppler vibrometer (LDV) aimed perpendicular to the sample surface. We use the Polytec OFV-505 sensor head with the OFV-5000 vibrometer controller. The sensor head emits a continuous-wave 632 nm HeNe laser which reflects off thin retroreflective tape applied to the sample surface. Due to the Doppler effect, the frequency of the reflected beam varies in proportion to the velocity of the ultrasonic vibrations. The ultrasonic waveform is decoded from the frequency modulated signal produced by combining the reflected beam with a reference beam inside the sensor head.[18] We use the DD-300 displacement decoder, which outputs the absolute displacement of the sample surface. Waveforms are digitized with a 16-bit AlazarTech ATS660 PCI oscilloscope card installed within the experiment control PC. The LDV detects vibrations with the highest S/N ratio when the beam is automatically focused on the sample surface, subtending a diameter of approximately 20 μm. By carefully positioning the sensor head and constraining the focus range of the beam, we avoid any loss in data quality caused by aiming the LDV beam through the optical window.[28]

Rock samples are prepared for ultrasonic experiments by coring cylindrical plugs from larger specimens. To maintain a positive net difference between the external confining stress and the pore fluid pressure, all rock samples are encapsulated with a thin brass jacket, preventing the ingress of nitrogen gas into the pores. The jacket consists of 38 μm thick brass shim applied to the rock surfaces with a uniform layer of approximately 20 μm thick epoxy. In Sec. III B, we show how the brass and epoxy jacket affects LUS measurements.

In order to take full advantage of the high spatial resolution of LUS measurements, the location of the laser beams on the surface of the sample must be readily adjustable. To accomplish this, previous LUS studies have employed rotational or linear stages.[14,15,17] In our apparatus, we achieve angular adjustment by vertically mounting the cylindrical rock samples on an inexpensive stepper motor inside the pressure vessel. We use a stepper motor (RS Pro brand) which moves at increments of $0.90° \pm 0.05°$, powered and controlled via four wires that are connected through a cable gland in the pressure vessel cap. Positioning and rotation are controlled with a stepper motor driver (L298N H-bridge) connected to an Arduino Uno microcontroller. The Arduino runs customized code which receives positioning commands through Universal Serial Bus (USB) from a computer or via manual input from an adjustable knob.

Instrument control and data acquisition are controlled with PLACE, the Python-based laboratory automation software package[29] (see https://github.com/palab/place for source code, documentation, and tutorials). Each instrument is represented as a module in a graphical user interface where the parameters for that instrument can be configured. These modules can be activated and deactivated depending on the specific instruments being used. An experiment consists of a series of updates where each instrument performs its task in sequence and returns any acquired data. At the completion of the experiment, data are saved into a single organized NumPy array

for ease of access, along with an experiment configuration file which allows the experiment to be easily repeated. A custom module was written for the Arduino-controlled stepper motor where the start position, end position, and/or step size can be set. Following data acquisition, processing and analysis is performed with the Python code specifically written to handle the large amount of waveform data produced in these experiments.[28]

III. RESULTS

In Secs. III A to III C, we present results of experiments to validate our *in situ* LUS methodology and demonstrate its capabilities. Section III A presents a control experiment comparing LUS data to conventional transducer data, while Sec. III B investigates the effect of the sample jacket on LUS measurements. Both of these experiments use a homogeneous 44.26 mm diameter aluminum cylinder as a near purely elastic standard with low attenuation properties.[30] In Sec. III C, we present two rock physics experiments which demonstrate the types of data that can be acquired with our apparatus. The results of these experiments are interpreted and discussed in Sec. IV.

A. Comparison with transducers

First, we compare the wavefield recorded with our LUS apparatus to that acquired with the well-established pulse transmission method using conventional transducers. The aluminum cylinder is oriented with its long axis vertical inside the pressure vessel, with the source and receiver laser beams aligned at diametrically opposite points. The recorded waveform is calculated by averaging 1000 realizations. Following the LUS data acquisition, two 0.5 MHz V101 Olympus transducers are aligned at the same locations as the source and receiver laser beams to acquire the transducer waveform. The one inch transducers are tangentially coupled to the aluminum cylinder with Magnaflux® Shear Gel. Figure 3 shows the comparison of the two waveforms, normalized by the maximum amplitude of the direct primary (P-)wave. The coincidence of first breaks confirms that our LUS apparatus records the same P-wave arrival time through the pressure vessel windows as the transducer pulse transmission experiment. The energy arriving after the first break in the LUS waveform corresponds to surface waves and scattered body waves that have significantly higher amplitudes than the direct P-wave. In the transducer waveform, the direct P-wave contains larger amplitudes than energy arriving at later times. Finally, we note that the earliest arriving energy in the LUS waveform is higher in frequency than in the transducer waveform.

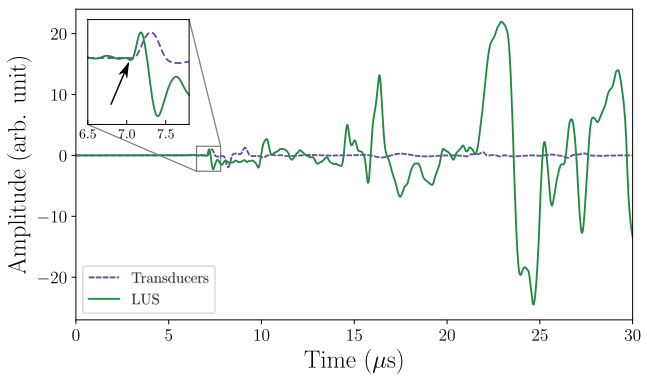

FIG. 3. Comparison of waveforms recorded on the aluminum cylinder using transducers and laser ultrasonics (LUS). The LUS waveform is recorded through the optical windows of the pressure vessel at atmospheric pressure. Both waveforms are normalized by the amplitude of the direct P-wave, and a high-cut filter is applied to remove instrument noise above 6 MHz. The manually picked arrival time of the P-wave (black arrow) is identical in both waveforms.

B. Effects of the sample jacket

Since both the generation and detection of ultrasound occurs on the surface, the effects of the jacket on the measurement of elastic waves need to be understood and accounted for. To test the effect of the jacket, we record LUS waveforms on the aluminum standard with and without the jacket. The source and receiver beams are aligned at diametrically opposite points on the cylinder which is mounted with its long axis vertical inside the pressure vessel. LUS data are recorded at 17 positions separated by 10° increments around the sample; the final waveforms represent the average of the data recorded at all positions.

Figure 4(a) shows a comparison of two waveforms recorded with and without the jacket at atmospheric pressure. The waveforms are similar in appearance for approximately the first 20 μs, after which time they gradually desynchronize. The jacket delays the direct P-wave by 0.04 μs, agreeing with the time delay predicted using quoted P-wave speeds through the respective thicknesses of brass and epoxy.[28] We subtract this small time delay when calculating absolute P-wave velocities from our LUS waveforms. Power spectral density plots calculated using the multitaper method[31,32] reveal that the jacket decreases the power recorded at all frequencies and that the reduction in power is greater for frequencies above 500 kHz compared to those below 500 kHz [Fig. 4(b)].

To understand how increasing temperature affects the time delay of the brass and epoxy jacket, we record waveforms on the aluminum cylinder with and without the jacket at temperatures between 20° and 150 °C and a constant pressure of 10 MPa. We observe a monotonic increase in the arrival time of the direct P-wave as temperature increases for both tests (Fig. 5). Without the jacket, the slope of the arrival time best-fit line is 0.014 ± 0.01 μs/10 °C, while the slope with the jacket is 0.020 ± 0.001 μs/10 °C, giving a difference of 0.006 ± 0.002 μs for every 10 °C increase in temperature.

C. Rock physics results

We now demonstrate the implementation of our *in situ* LUS apparatus through two rock physics experiments. For these experiments, we study an ultramylonite rock from the Alpine Fault, a major oblique transform plate boundary fault that separates the Pacific and Australian Plates along the length (>600 km) of the South Island in New Zealand.[33] The sample was collected from a surface outcrop near the fault. Rapid rock exhumation at the Alpine Fault (30 km in 3 M years) means ultramylonites collected at the surface are unweathered and representative of depths up to 30 km.[34] The rock is cored to a diameter of 25.08 mm and cut to a length of

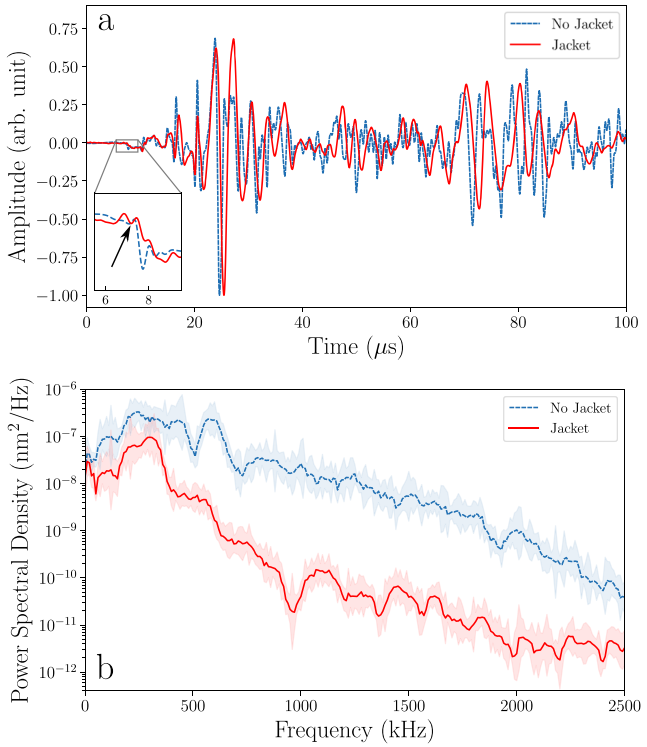

FIG. 4. Comparisons of waveforms (a) and power spectral densities (b) of the aluminum at atmospheric pressure with and without the brass and epoxy jacket. A low-pass filter with a corner frequency of 2 MHz is applied to the waveforms in (a) to remove instrument noise. Amplitudes are normalized by the maximum displacement, and the black arrow indicates the manually picked direct P-wave arrival time. Shaded regions in (b) denote the 90% confidence intervals for the multitaper spectral estimates.

25.19 mm, with the plane of visible foliation aligned with the long axis of the cylinder. A brass jacket is applied to the rock surface, and the sample is mounted inside the pressure vessel with the long axis of the cylinder aligned vertically.

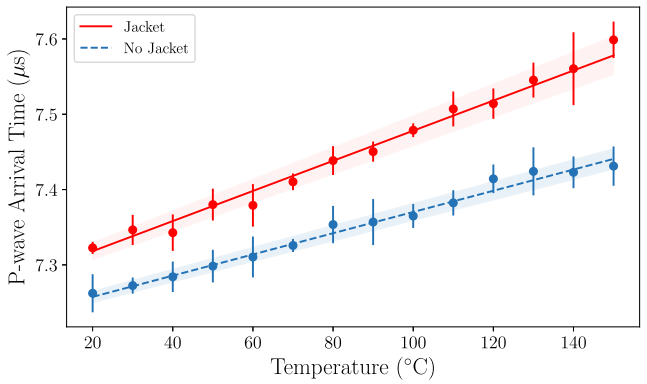

FIG. 5. P-wave arrival time picks for the aluminum cylinder with and without the jacket at different temperatures. Least-squares lines are fitted to the arrival times, with the shaded regions denoting uncertainty in the fit.

1. Rotational scans under pressure

In our first experiment, we utilize the rotational stage to record the wavefield with different source and receiver positions around the rock sample. With the source and receiver positions fixed at diametrically opposite sides of the sample, ultrasonic waveforms are acquired at 1.8° rotational increments over an angular range of 165.6°. To increase the S/N ratio, the waveform at each position is the average of 200 pulses of the source laser; these waveforms are sampled by the oscilloscope card at a rate of 50 MHz. Rotational scans are recorded at atmospheric pressure and 16 MPa, which corresponds to a subsurface depth of approximately 1 km.

The full rotational scan wavefields are visualized in Fig. 6. In each of the two plots, the waveforms are transformed to display true amplitude in a color scale with angular position on the horizontal axis and time on the vertical axis. Following the methodology of Maeda and Naoki,[35] the arrival times of the P-wave first breaks were automatically picked with the Akaike Information Criterion (AIC) method, a robust autoregressive picking algorithm that reliably and rapidly identifies the P-wave arrivals for large LUS datasets.[28] Figure 6 shows that the arrival of the first compressional wave varies sinusoidally as a function of angle for both scans. The earliest P-wave arrival occurs at 20°, while the latest P-wave arrival occurs when the sample is rotated by 90°, at 110°. Scattered compressional waves arrive after the first direct P-wave, followed by a series of large-amplitude waves after approximately 20 μs in the atmospheric pressure scan and 15 μs in the 16 MPa scan. These arrivals represent evanescent surface waves propagating around the circumference of the sample. In the atmospheric pressure scan, the peak of the surface wave follows a similar sinusoidal variation to the P-wave between 23 μs and 27 μs, while at 16 MPa the surface wave is mostly time invariant with angular orientation at ~17 μs.

A striking feature in these wavefields is the marked difference of the P-wave arrival times between the two pressures, as seen in the arrival time curves in Fig. 6(a). At atmospheric pressure, the difference between the earliest and latest P-wave arrival times is 6.30 μs, while at 16 MPa, this difference reduces to 2.66 μs. Moreover, the P-wave arrival time in the fast direction decreases by 5% with the increase in pressure, while the arrival time in the slow direction decreases by 65% over the same pressure range. This corresponds to an overall reduction in P-wave velocity anisotropy[36] from 62% at atmospheric pressure to 36% at 16 MPa. Finally, Fig. 6(b) shows that the amplitudes of both the first-arriving P-waves and body waves decrease as the pressure is increased.

2. In situ temperature scans

The second experiment compares ultrasonic waveforms on the ultramylonite sample between 20 °C and 100 °C. The sample is mounted inside the pressure vessel in the same way as the rotational scans, but the orientation of the source-receiver geometry is fixed in the slow direction, perpendicular to the foliation in the sample. Temperature is increased over a period of approximately 6 h, with ultrasonic waveforms recorded at increments of 10 °C. All waveforms are recorded at a confining stress of 10 MPa (~650 m depth). The temperature range represents typical *in situ* temperatures within the upper 1 km of crust near the Alpine Fault, where the geothermal gradient is unusually high (125 ± 55 °C per km[37]).

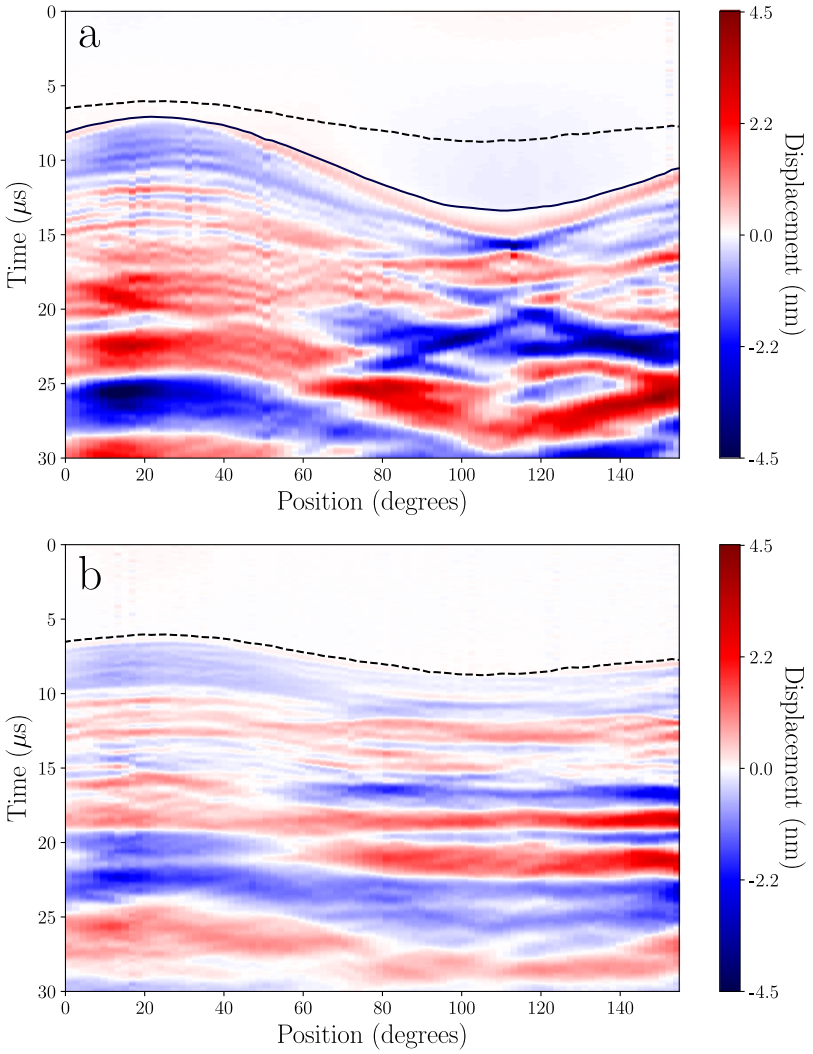

FIG. 6. Wavefields of scans recorded at (a) atmospheric pressure and (b) 16 MPa for an ultramylonite sample. Time is recorded from the pulse laser firing, and colors show the absolute displacement of the sample surface as recorded by the LDV. The solid black line denotes the arrival of the direct P-wave in the atmospheric pressure scan, while the dashed black lines show the P-wave arrival time at 16 MPa. The data have been bandpass filtered between 20 kHz and 3 MHz to remove instrument noise.

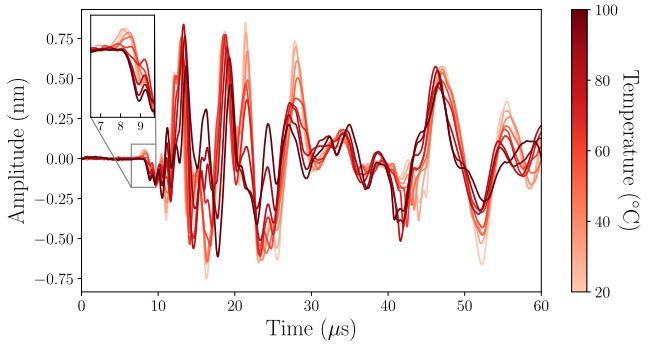

FIG. 7. Waveforms recorded at different rock temperatures in the slow P-wave direction of the rock sample. The confining stress was held constant at 10 MPa. The small time delay caused by the sample jacket has been subtracted.

In general, both the amplitude and arrival time of common phases decrease as the temperature increases (Fig. 7). Between 20 °C and 100 °C, the direct P-wave arrival time increases from 7.60 μs to 8.05 μs, corresponding to a 5.6% decrease in P-wave velocity.

IV. DISCUSSION

We have developed the first methodology capable of acquiring noncontact laser ultrasonic measurements of rock samples under *in situ* subsurface confining pressures and temperatures. The results presented here demonstrate the capability of our apparatus to produce valuable rock physics datasets.

Comparisons of LUS data to a conventional transducer waveform show that both methods measure the same P-wave arrival time. The waves thereafter in Fig. 3 represent scattered body waves and surface waves. Variations in the relative amplitudes between the LUS

and transducer data are caused by differences in the source and receiver characteristics. Contacting P-wave transducers efficiently generate on-axis longitudinal waves, while the thermoelastic source is less efficient for generating such particle motion.[18] Another reason why the surface waves are larger relative to the P-wave in the LUS setup is the difference in sensor footprint. The transducers cover an area of the sample that is roughly the size of a wavelength, meaning surface waves interfere destructively.[18] Moreover, the broadband generation and detection characteristics of the LUS lasers give rise to the higher frequencies in the LUS waveform. Despite these relative amplitude and frequency content differences, the comparison demonstrates that the LUS setup accurately records ultrasonic waveforms through the pressure vessel windows.

Figure 4 demonstrates that the brass sample jacket affects the frequency content. Reduced power is likely caused by a lower efficiency of the conversion of infrared light to ultrasound in brass compared to aluminum.[18] Also, acoustic impedance contrasts between the brass, epoxy, and aluminum decrease the transmission of ultrasound into the sample, and attenuation of surface waves within the epoxy layer reduces the power at higher frequencies. Since the acoustic impedances of aluminum and rocks are similar, we expect similar frequency content and amplitude effects when the jacket is applied to rock samples. In addition, the propagation time of a direct P-wave through the sample jacket is 0.04 μs. As travel time increases, the extra propagation distance through the jacket of successive waves also increases. Further validation tests with the aluminum cylinder under confining stresses up to 14 MPa confirmed that the frequency content, amplitude, and lag time effects from the jacket are invariant with pressure.[28] Thus, while the jacket clearly influences the generation and propagation of ultrasound, these differences do not affect qualitative and quantitative comparisons between waveforms recorded with the jacket.

Control tests on the aluminum cylinder with and without the jacket at different temperatures (Fig. 5) show that the P-wave arrival time increases monotonically as temperature increases. For the data recorded without the jacket, this increase is caused by a combination of thermal expansion of the aluminum and reduction in the P-wave velocity with temperature. Thus, the increase in the arrival time delay caused by the jacket is described by the difference in the slopes of the best-fit lines in Fig. 5 (0.006 ± 0.002 μs for every 10 °C increase in temperature). This increasing delay is likely caused by the expansion of the brass and softening of the epoxy and can be corrected for in the arrival times of high-temperature experiments.

The rotational scan data of the Alpine Fault ultramylonite reveals strong P-wave velocity anisotropy which decreases from 62% at atmospheric pressure to 36% at 16 MPa. The angular dependence of P-wave velocity in this rock sample is controlled by the preferred alignment of platy minerals and planar microcracks.[28] The fast P-wave direction is oriented parallel to the plane of mineral layering, while the slow direction is oriented perpendicular to the layering. However, the strong pressure dependence of the anisotropy indicates that the degree of anisotropy is largely controlled by the microcracks, rather than the minerals. As the pressure increases, the planar microcracks close in a direction perpendicular to the layering, dramatically increasing the elastic stiffness of the rock, and hence the P-wave velocity, in the slow direction. On the other hand, the stiffness of the rock remains relatively constant in the fast direction as the pressure increases. The observed strong pressure dependence highlights the importance of acquiring rock physics data under *in situ* confining stress.

Similar pressure dependence of anisotropy has been commonly observed in fractured anisotropic rocks measured using the pulse transmission method.[7,24,38,39] However, our LUS methodology allows us to acquire an order of magnitude more independent P-wave velocity estimates at different angles around the sample compared to traditional methods. This enables the orientation of the fast and slow directions to be determined experimentally, rather than assumed before the rock samples are prepared. Moreover, the symmetry of the anisotropy (e.g., transverse, orthorhombic, etc.) can be tested rather than assumed. Finally, the elastic constant c_{13} can be accurately determined by fitting a curve to many estimates of the azimuthal P-wave velocity (this parameter describes the angular variation of P-wave velocity and is important for constructing accurate subsurface seismic velocity models[28]). Previous studies demonstrating similar improvements in anisotropy estimates have so far only reported measurements at atmospheric pressure[15,17] or with contacting transducers.[9,40] With our new methodology, we can now exploit all the advantages of noncontact LUS for quantifying the elastic anisotropy of rocks under *in situ* confining stress.

With the capability to record absolute displacements using the LDV, we observe an overall decrease in amplitude between the atmospheric pressure and 16 MPa scans (Fig. 6). Attenuation decreases as microcracks close,[41] suggesting that the reduction in amplitudes with increasing pressure is not due to changes within the rock. Rather, we suggest that as pressure is increased, more surface wave energy is radiated into the pressurized gas due to the reduced impedance contrast.[28] If this effect is accounted for, the absolute displacements recorded by the LDV could be used for detailed studies of attenuation or ultrasonic strain.

Measurements between 20° and 100 °C at 10 MPa confining stress reveal a 5.6% decrease in the P-wave velocity as temperature increases (Fig. 7). This behavior is consistent with the temperature dependence previously observed for other rocks.[1,23] Interestingly, the appearance of the P-wave first break changes as temperature increases. While this is partly due to the reduction in P-wave amplitude caused by softening of the epoxy and variations in the thermoelastic generation, it is possible that variations in amplitude could be caused by changes within the rock. Further experiments are planned in order to fully explain the behavior and mechanisms of the temperature dependence of Alpine Fault rocks. However, this initial test demonstrates the capability of our apparatus for performing ultrasonic wave measurements on rocks under both *in situ* confining stress and temperature.

Along with obtaining improved estimates of anisotropy, this apparatus can be used to acquire a wide range of improved and novel data for investigating rock and material elasticity under various temperature and pressure conditions. Examples include analyzing coda waves to detect very small changes in the velocity of rocks caused by microscale healing processes[42] or studying variations in the elastic properties of ice.[43,44]

V. CONCLUSIONS

We have developed the first apparatus to perform fully noncontact ultrasonic compressional wave measurements on rock samples

under *in situ* pressure and temperature conditions. This methodology offers several advantages over traditional transducer measurements. These include the absence of mechanical coupling, the small sampling area, and the broadband recordings of absolute displacement. Our results validate the methodology for acquiring accurate ultrasonic waveform data. Furthermore, rotational scans of an Alpine Fault ultramylonite rock show a significant decrease in anisotropy from 62% at atmospheric pressure to 36% at 16 MPa confining pressure. This result highlights the importance of performing rock measurements under *in situ* confining stress and demonstrates the advantages of the methodology for investigating elastic anisotropy. In addition to *in situ* pressure, our setup also allows us to investigate the temperature dependence of the elastic properties of rocks. In the ultramylonite sample, the P-wave speed decreases by 5.6% from 20 °C to 100 °C. In the future, we intend to further develop the methodology, expanding its capabilities for acquiring novel datasets to investigate ultrasonic wave propagation and elasticity in rocks and other materials under *in situ* conditions.

ACKNOWLEDGMENTS

We thank Paul Freeman and Jami Shepherd for their work in developing PLACE and Samuel Hitchman for his contribution to the development and operation of the apparatus. L.A. acknowledges support from the Royal Society of New Zealand under Marsden Grant No. 14-UOA-028. We also thank Alison Malcolm and an anonymous reviewer for their constructive comments, which helped improve this manuscript.

REFERENCES

[1] Z. Z. Wang, Geophysics **66**, 398 (2001).
[2] G. Mavko, T. Mukerji, and J. Dvorkin, *The Rock Physics Handbook: Tools for Seismic Analysis in Porous Media* (Cambridge University Press, 2003).
[3] B. Carpenter, H. Kitajima, R. Sutherland, J. Townend, V. Toy, and D. Saffer, Earth Planet. Sci. Lett. **390**, 45 (2014).
[4] M. J. Allen, D. Tatham, D. R. Faulkner, E. Mariani, and C. Boulton, J. Geophys. Res.: Solid Earth **122**, 6160, https://doi.org/10.1002/2017jb014355 (2017).
[5] F. Birch, J. Geophys. Res. **65**, 1083, https://doi.org/10.1029/jz065i004p01083 (1960).
[6] K. W. Winkler and T. J. Plona, J. Geophys. Res.: Solid Earth **87**, 10776, https://doi.org/10.1029/jb087ib13p10776 (1982).
[7] L. Vernik and A. Nur, Geophysics **57**, 727 (1992).
[8] J. Dellinger and L. Vernik, Geophysics **59**, 1774 (1994).
[9] J. Sarout, C. Delle Piane, D. Nadri, L. Esteban, and D. N. Dewhurst, Geophysics **80**, A19 (2015).
[10] H. Cho, S. Ogawa, and M. Takemoto, NDT&E Int. **29**, 301 (1996).
[11] M. Silva, R. Gouyon, and F. Lepoutre, Ultrasonics **41**, 301 (2003).
[12] J. L. Johnson, M. Merrilees, J. Shragge, and K. van Wijk, Photoacoustics **9**, 62 (2018).
[13] J. A. Scales and A. E. Malcolm, Phys. Rev. E **67**, 046618 (2003).
[14] K. van Wijk, J. Simpson, and S. Hitchman, Wave Motion **89**, 57 (2019).
[15] T. E. Blum, L. Adam, and K. van Wijk, Geophysics **78**, C25 (2013).
[16] J. Xie, J. Wei, B. Di, K. Xu, and Y. Chen, J. Geophys. Eng. **13**, 984 (2016).
[17] J. Xie, B. Di, D. R. Schmitt, J. Wei, and Y. Chen, Geophysics **83**, C137 (2018).
[18] C. B. Scruby and L. E. Drain, *Laser Ultrasonics: Techniques and Applications* (Adam Hilger, Bristol, 1990).
[19] B. Pouet and P. N. J. Rmolofosaon, *SEG Technical Program Expanded Abstracts 1990* (Society of Exploration Geophysicists, 1990), pp. 841–844.
[20] R. J. Dewhurst, C. Edwards, A. D. W. McKie, and S. B. Palmer, J. Appl. Phys. **63**, 1225 (1988).
[21] K. L. Telschow, J. B. Walter, and G. V. Garcia, J. Appl. Phys. **68**, 6077 (1990).
[22] C. Scruby and B. Moss, NDT&E Int. **26**, 177 (1993).
[23] D. S. Hughes and J. H. Cross, Geophysics **16**, 577 (1951).
[24] K. Ullemeyer, T. Lokajíček, R. N. Vasin, R. Keppler, and J. H. Behrmann, Phys. Earth Planet. Inter. **275**, 32 (2018).
[25] M. Lebedev, A. Bóna, R. Pevzner, and B. Gurevich, Geophysics **76**, WA83 (2011).
[26] M. Carson and M. Lebedev, *SEG Technical Program Expanded Abstracts 2014* (Society of Exploration Geophysicists, 2014), pp. 2755–2759.
[27] L. Adam, F. Ou, L. Strachan, J. Johnson, K. van Wijk, and B. Field, *SEG Technical Program Expanded Abstracts 2014* (Society of Exploration Geophysicists, 2014), pp. 2749–2754.
[28] J. Simpson, "Non-contact measurements to estimate the elastic properties of rocks under in situ conditions," M.Sc thesis, The University of Auckland, 2019.
[29] J. L. Johnson, H. tom Wörden, and K. van Wijk, J. Lab. Autom. **20**, 10 (2015).
[30] J. Zemanek and I. Rudnick, J. Acoust. Soc. Am. **33**, 1283 (1961).
[31] G. A. Prieto, R. L. Parker, and F. L. Vernon III, Comput. Geosci. **35**, 1701 (2009).
[32] L. Krischer, mtspec Python wrappers 0.3.2 (Data set), 2016.
[33] R. J. Norris and A. F. Cooper, J. Struct. Geol. **23**, 507 (2001).
[34] R. J. Norris and A. F. Cooper, in *A Continental Plate Boundary: Tectonics at South Island, New Zealand*, edited by D. Okaya, T. Stern, and F. Davey (American Geophysical Union, 2007), pp. 157–175.
[35] N. Maeda, Zisin (J. Seismol. Soc. Jpn. 2nd Ser.) **38**, 365 (1985).
[36] P-wave anisotropy is calculated using the formula $A_P = (V_f - V_s)/[0.5(V_f + V_s)]$, where V_f and Vs are the fast and slow P-wave velocities.
[37] R. Sutherland, J. Townend, V. Toy, P. Upton, J. Coussens, M. Allen, L.-M. Baratin, N. Barth, L. Becroft, C. Boese, A. Boles, C. Boulton, N. G. R. Broderick, L. Janku-Capova, B. M. Carpenter, B. Célérier, C. Chamberlain, A. Cooper, A. Coutts, S. Cox, L. Craw, M.-L. Doan, J. Eccles, D. Faulkner, J. Grieve, J. Grochowski, A. Gulley, A. Hartog, J. Howarth, K. Jacobs, T. Jeppson, N. Kato, S. Keys, M. Kirilova, Y. Kometani, R. Langridge, W. Lin, T. Little, A. Lukacs, D. Mallyon, E. Mariani, C. Massiot, L. Mathewson, B. Melosh, C. Menzies, J. Moore, L. Morales, C. Morgan, H. Mori, A. Niemeijer, O. Nishikawa, D. Prior, K. Sauer, M. Savage, A. Schleicher, D. R. Schmitt, N. Shigematsu, S. Taylor-Offord, D. Teagle, H. Tobin, R. Valdez, K. Weaver, T. Wiersberg, J. Williams, N. Woodman, and M. Zimmer, Nature **546**, 137 (2017).
[38] M. S. King, Geophysics **31**, 50 (1966).
[39] Z. Wang, Geophysics **67**, 1423 (2002).
[40] F. Yan, D.-h. Han, and Q. Yao, *SEG Technical Program Expanded Abstracts 2014* (Society of Exploration Geophysicists, 2014), pp. 2983–2987.
[41] D. H. Johnston and M. N. Toksov, J. Geophys. Res. **85**, 925, https://doi.org/10.1029/jb085ib02p00925 (1980).
[42] A. Grêt, R. Snieder, and J. Scales, J. Geophys. Res.: Solid Earth **111**, B03305, https://doi.org/doi:10.1029/2004jb003354 (2006).
[43] M. J. Vaughan, K. van Wijk, D. J. Prior, and M. H. Bowman, Cryosphere **10**, 2821 (2016).
[44] T. Mikesell, K. van Wijk, L. Otheim, H.-P. Marshall, A. Kurbatov, T. D. Mikesell, K. Van Wijk, L. T. Otheim, H.-P. Marshall, and A. Kurbatov, Geosciences **7**, 47 (2017).